Magnetic imaging with full-field soft X-ray microscopies

Peter Fischer[a,], Mi-Young Im[a], Chloe Baldasseroni[b], Catherine Bordel[c, d], Frances Hellman[c, d], Jong-Soo Lee[e], Charles S. Fadley[f, d]
[a] Center for X-ray Optics, Lawrence Berkeley National Laboratory, 1 Cyclotron Road, Berkeley, CA 94720, USA
[b] Department of Materials Science and Engineering, University of California Berkeley, Berkeley, CA 94720, USA
[c] Department of Physics, University of California Berkeley, Berkeley, CA 94720, USA
[d] Material Sciences Division, Lawrence Berkeley National Laboratory, Berkeley, CA 94270, USA
[e] Department of Energy Systems Engineering, Daegu Gyeongbuk Institute of Science and Technology (DGIST), Daegu 711-873, South Korea
[f] Department of Physics, University of California Davis, Davis, CA 95616, USA

Abstract

Progress toward a fundamental understanding of magnetism continues to be of great scientific interest and high technological relevance. To control magnetization on the nanoscale, external magnetic fields and spin polarized currents are commonly used. In addition, novel concepts based on spin manipulation by electric fields or photons are emerging which benefit from advances in tailoring complex magnetic materials. Although the nanoscale is at the very origin of magnetic behavior, there is a new trend toward investigating mesoscale magnetic phenomena, thus adding complexity and functionality, both of which will become crucial for future magnetic devices.

Advanced analytical tools are thus needed for the characterization of magnetic properties spanning the nano- to the meso-scale. Imaging magnetic structures with high spatial and temporal resolution over a large field of view and in three dimensions is therefore a key challenge. A variety of spectromicroscopic techniques address this challenge by taking advantage of variable-polarization soft X-rays, thus enabling X-ray dichroism effects provide magnetic contrast. These techniques are also capable of quantifying in an element-, valence- and site-sensitive way the basic properties of ferro(i)- and antiferro-magnetic systems, such as spin and orbital moments, spin configurations from the nano- to the meso-scale and spin dynamics with sub-ns time resolution.

This paper reviews current achievements and outlines future trends with one of these spectromicroscopies, magnetic full field transmission soft X-ray microscopy (MTXM) using a few selected examples of recent research on nano- and meso-scale magnetic phenomena. The complementarity of MTXM to X-ray photoemission electron microscopy (X-PEEM) is also emphasized.

1. Introduction

Magnetic materials are the backbone of many key technologies, ranging from information and sensor technologies to transportation, power generation and conversion. A fundamental understanding of magnetic properties on the nanoscale is not only scientifically challenging, since it addresses the spins of correlated electrons, but is also of paramount importance for novel concepts and advanced technological applications [1] and [2]. A prototypic example for the intimate connection between scientific achievements and technological applications is the discovery of Giant Magnetoresistance (GMR), which not only contributed strongly to a profound understanding of the spin-dependent scattering of electrons in thin magnetic films, but had also a tremendous impact on the achievements in magnetic storage technologies immediately after its first discovery [3], [4] and [5].

One of the primary goals in nanomagnetism research is to control spins on the nanoscale and there are several ways to do this. The field of spintronics exploits those mechanisms to develop new technological concepts based on the spin of the electron. Whereas the application of external magnetic fields (Oersted fields), which forces the magnetic moments to align parallel to the field direction, is still the basic concept to write information in a magnetic storage element, novel effects, using the local torque which is exerted by the electron spins in a spin-polarized current are intensely being studied, and have in fact recently been utilized in a commercial device [6] and [7]. Alternatively, in multiferroic materials, where multiple degrees of freedom, such as ferroelectricity and ferromagnetism, coexist, it has been shown that spins can be controlled by electric fields [8] and [9]. Unfortunately, there are not too many naturally occurring multiferroic systems, and therefore multiferroic materials are an intense topic in materials sciences, where advanced synthesis techniques are utilized and developed to artificially fabricate such materials. Since multiferroic behavior is often induced by strain, “straintronics” has recently become a very active research area [10].

To understand magnetic properties on the nanoscale, advanced characterization tools are mandatory, and these should meet the following requirements:

-*spatial* resolution below 10 nm,

-*temporal* resolution down to the fsec regime,

-*chemical* and *magnetic* sensitivity with *elemental specificity*.

The first two requirements reflect the fundamental length and time scales of magnetism, while the last is a consequence of the fact that multicomponent materials can offer properties which differ from those of single-phase materials, thus motivating a “materials-by-design” approach. The first two requirements are related to the exchange interaction of individual spins, which is the strongest interaction in magnetic materials. Magnetic *exchange lengths*, which are largely determined by characteristic, i.e. material-specific, constants for exchange and anisotropy energies, are typically in the

sub-10 nm range. The corresponding fundamental *time scale* for the exchange interaction, the exchange time, which can be derived from the Heisenberg uncertainty principle between time and energy, yields several tens of fsec. For comparison, typical time scales for the spin–orbit interaction have values in the psec regime, which are relevant for understanding, e.g. the dynamics of anisotropies. The time scales which govern, e.g. dipolar interactions or precessional motion of spins are in the nsec regime.

A multitude of magnetic characterization techniques has been developed in the past; however the utilization of soft X-ray spectromicroscopies offers a unique combination of relevant features and those are therefore among the most promising probes for nanoscale magnetic studies.

The uniqueness of soft X-rays for magnetism studies is intimately connected to their wavelength, photon energy and time structure, as well as their intensity and polarization characteristics [11]. With a wavelength spanning from about 5 nm to 0.5 nm, the diffraction limit, which corresponds to an inherent limit in spatial resolution or correlation length scales, is in the few nanometer regime. The corresponding photon energy between about 200 eV and 2 keV matches the inner core electron binding energies, which in turn give raise to an element-specific increase in X-ray absorption for those specific X-ray absorption edges. In particular, the L edges of 3d transition metals such as Fe, Co and Ni, as well as the M edges of rare earth elements happen to be in that regime. At current soft X-ray sources, such as synchrotron storage rings, the polarization of soft X-rays can be tuned from circular to elliptical and linear by dedicated sources, which allows using magnetic X-ray dichroism effects. They can be seen as the X-ray counterparts of well-known magneto-optical effects, such as the Kerr [12] and Faraday [13] effects, with the former referring to reflection, and the latter to absorption geometries). However, the soft X-ray analogs provide inherent elemental specificity and much larger magnetic cross-sections due to the strong spin–orbit coupling at the L_2 and L_3 (or M_4 and M_5) spin–orbit coupled X-ray absorption edges [14]. The application of magneto-optical sum rules to the X-ray magnetic circular dichroism (XMCD) effect further permits quantitatively extracting from XMCD spectroscopic data both the spin and orbital magnetic moments [15] and [16]. Lastly, synchrotron storage rings deliver burst of X-ray pulses, which provide an inherent time structure to those X-ray sources. Typically, at third generation sources, such as the Advanced Light Source (ALS) in Berkeley, these X-ray pulse lengths are in the <100 ps regime, but the next generation of X-ray sources, such as X-ray free electron lasers at the Linear Coherent Light Source (LCLS) in Stanford or the FLASH facility in Hamburg/Germany can now generate fsec short X-ray pulses with a peak brilliance which is orders of magnitude higher than what can be achieved today. For example, typical current X-ray fluxes are at about 10^{12} ph/s, whereas XFELs can produce about 10^{13} ph in a few fsec. Thus, exciting new opportunities for using soft X-rays in studies of magnetic materials are opening up.

While the understanding of nanoscale magnetic behavior is crucial and serves as the building block for novel magnetic devices, mesoscale systems have also recently received a significant interest. The mesoscale is not just defined as a length scale which bridges the nanoscale, i.e. the length scale of single atoms – to the microscopic range,

where the magnetic properties act as a continuum, but it also adds complexity, stochasticity and functionality. It can be anticipated that effects which are related to those phenomena will see an increased relevance in future applications and will probably require new and extended theoretical models that bridge nanoscale and mesoscale behavior.

Complexity in magnetic materials will also become more important not only in multi-component combinatorial materials design approaches, such as the “materials genome initiative” [17], which aims to discover and tailor specific properties from basic principle calculations of novel materials, but also in devices extending into the third dimension, where the “simple” cross-talk in more common planar geometries will turn into corresponding volume effects. Related to this is the importance of interfaces, which play a crucial role in multi-component systems. The question of whether a specific magnetic process on the nano- or the meso-scale is fully deterministic or follows a *stochastic* behavior is not only scientifically fundamental, but moreover of utmost technological importance. Lastly, a steady-state characterization can only provide information about the static structure, but the *functionality*, e.g. of a magnetic device can only be understood if one is able to characterize the fast and ultrafast spin dynamics of a magnetic system, with high spatial resolution from the nano- to the meso-scale.

Imaging magnetic structures in three dimensions and in their corresponding fast and ultrafast spin dynamics in novel and advanced magnetic materials is thus not only a very appealing analytical approach [18], but it also provides detailed insight into magnetic behavior. Already, a variety of magnetic imaging techniques has been developed which permit studying static domain structures, i.e. the spin configuration in thermal equilibrium at highest spatial resolution. These techniques make use of various probes interacting with the magnetic material.

There are also optical microscopes using the magneto-optical Kerr effect (MOKE) [19], where a contrast is generated by the rotation of the polarization vector of the incoming light by a magnetic moment and where the utilization of ultrafast optical laser pulses has achieved a very fast (fsec) time resolution [20], albeit at moderate (diffraction limited) spatial resolution only.

There are electron microscopes, such as the Lorentz transmission electron microscope (TEM) [21], which utilizes the Lorentz force diverting the electrons as they propagate through the magnetic specimen, the Scanning Electron Microscope with subsequent Polarization Analysis of the electrons (SEMPA) [22], or the spin polarized low energy electron microscopy (SPLEEM) [23]. The X-ray photoemission electron microscopy (PEEM), which is one of the X-ray imaging techniques delineated in this review, can be seen as a hybrid between electron microscopies and X-ray microscopies, taking advantage of the limited escape depth of electrons in solid, which provides strong surface sensitivity [24].

There is also a variety of scanning probe microscopes, such as the Magnetic Force Microscope (MFM) [25], which senses the interaction of the stray field emanating from

the sample onto its magnetic tip or the Spin Polarized Scanning Tunneling Microscope (SP-STM) [26], which detects the tunneling current between a magnetic tip and the sample's surface. Among the magnetic microscopy techniques, the SP-STM leads in spatial resolution as it has so far achieved almost atomic resolution.

In the following we will principally review full-field soft X-ray microscopies, in particular magnetic full-field transmission soft X-ray microscopy (MTXM) [27], which utilizes state-of-the-art Fresnel zone-plate optical elements for imaging, and permits studying mesoscale magnetic phenomena down to about 10–20 nm resolution. Examples from recent research will elucidate the information which can be obtained in terms of spatial and temporal resolution, and element specificity, as well as complexity, stochasticity and functionality. We will also briefly discuss the complementarity of MTXM to X-ray photoemission electron microscopy (X-PEEM) [24].

2. Experimental

Although X-rays were discovered by W.C. Roentgen in 1885, the lack of appropriate X-ray optics prevented doing true X-ray microscopy for nearly 100 years. However, in the mid-1980s, it was realized that Fresnel zone plates (FZP), which are circular gratings with a radially increasing line density, can be used as diffractive optics to build X-ray microscopes and the concurrent maturity of nanotechnological tools such as e-beam lithography then enabled the fabrication of high quality X-ray optics, which are now readily available. For an overview of the current status of X-ray microscopy, we refer to [28].

FZPs can be designed and customized for specific purposes and applications. The key design parameters are Δr, which is the outermost ring diameter, N, the number of zones, and λ, the photon wavelength at which the FZP is operating, and one obtains finally a spatial resolution which is proportional to Δr, a focal length $\sim 4N(\Delta r)^2/\lambda$ and a spectral bandwidth which is $\sim 1/N$. The latest generation of FZP optics used in soft X-ray microscopes has demonstrated a spatial resolution of better than 10 nm [29] (Fig. 1).

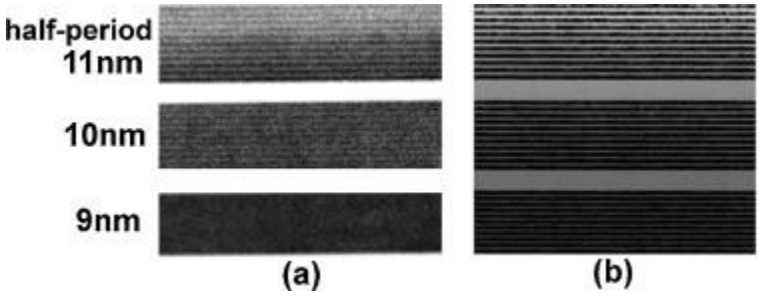

Fig. 1. (a) Soft X-ray transmission microscopy image taken at 1.75 nm wavelength (708 eV photon energy) and (b) transmission electron image of a test object (Mo/Si multilayer) showing that 10 nm lines and spaces could be resolved with Fresnel zone plate optics.

From Ref. [29].

The optical setup of the full-field soft X-ray microscope end-station XM-1, located at the ALS in Berkeley, CA (where the TXM data presented in this review have been obtained) is shown in Fig. 2. Details of this instrument are described elsewhere [30]. The principle of this instrument follows that of an optical microscope. The main components are (a) a light source, which is the bending magnet source at a third generation X-ray synchrotron such as the ALS; (b) a first FZP, acting as a condenser lens, (CZP), and a combined monochromator and illuminating optic; (c) a high resolution objective lens, the micro zone plate (MZP); and (d) a two-dimensional detector, which is a commercially available charge-coupled-device (CCD) system. The spectral resolution achievable with XM-1 is dominated by the CZP-pinhole arrangement, whereas the spatial resolution is set largely by the MZP in use. Some typical values under real operating conditions as presented below are 706 and 719 eV for the L_3 and L_2 edges of Fe as a typical 3d transition metal, about 20 nm spatial resolution, about 1 eV spectral resolution and (in time-resolved mode) 70 ps temporal resolution.

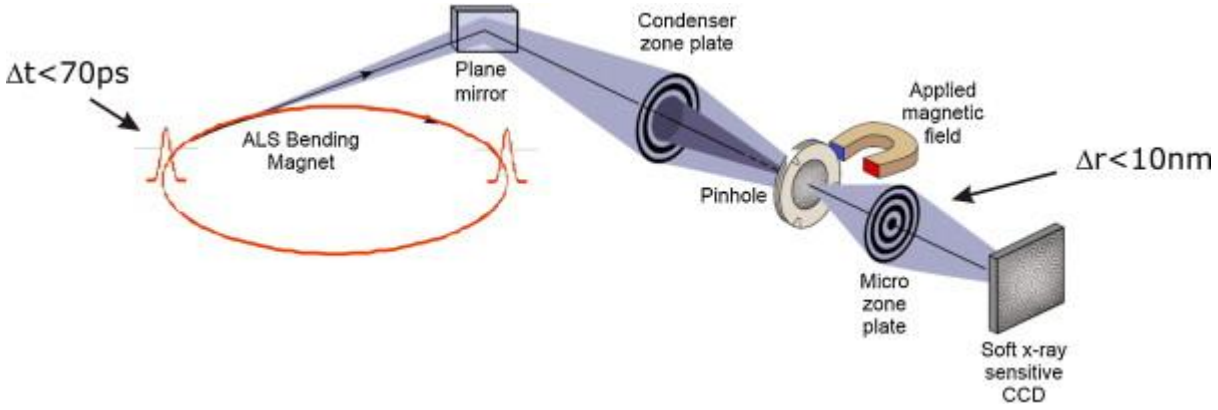

Fig. 2. Schematics of the optical setup of the full field soft X-ray transmission microscope XM-1 located at beamline 6.1.2 at the Advanced Light Source.

From Ref. [30].

Complementary to MTXM is the widely used X-ray photoemission electron microscope (X-PEEM) technique. Fig. 3 shows the schematics of an X-ray PEEM instrument [31]. In most of these instruments, the low-energy secondary electrons generated in the primary X-ray absorption process are used for imaging, leaving the sample through the surface and being guided through a high-resolution electron optics column onto the imaging detector. Also available, and with an increasing number of commercial sources, are X-PEEMs that can also do energy filtering so as to image with true photoelectrons that can be associated with the individual electronic states in the sample. The latest generation of X-PEEM instruments incorporates an aberration correction scheme, which aims for a sub-10 nm spatial resolution.

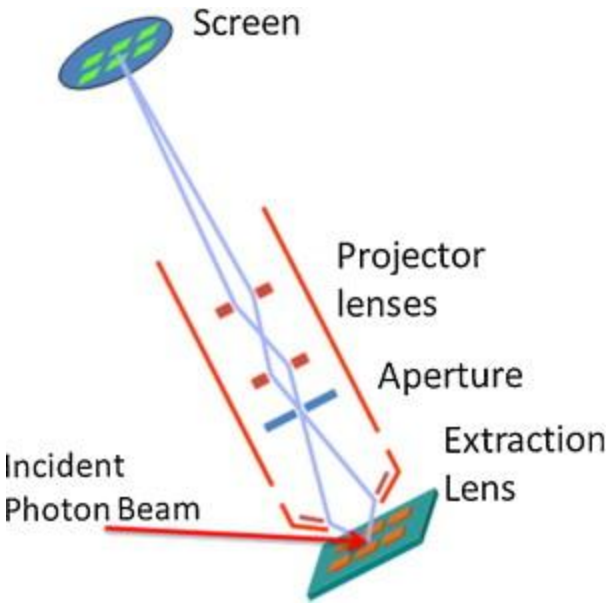

Fig. 3. Schematics of an X-PEEM system.

From Ref. [31].

The accessible range of photon energies determines which core levels of the elements can be addressed by these various instruments. The specific ALS instrument XM-1 was originally designed for biological imaging and offers a fairly limited photon range between about 500–1100 eV, but the next-generation TXMs fed by high-brightness undulator sources will expand this significantly [32].

To obtain magnetic contrast with polarized soft X-rays one most often utilizes the effect of X-ray magnetic circular dichroism (XMCD). XMCD describes the strong dependence of the absorption of circularly polarized X-rays on the relative orientation between the photon helicity and the magnetization axis in the sample. The XMCD effect occurs predominantly in the vicinity of the X-ray absorption edges, such as the spin–orbit coupled L_2 and L_3 edges. Those reflect the element-specific binding energies of inner core electrons, and thus XMCD adds an inherent elemental magnetic sensitivity to X-ray spectroscopies and microscopies, in particular to the transmission soft X-ray microscopy (TXM) and X-PEEMs described here. Large XMCD effects with values up to 25% occur, e.g. for the L edges of 3d transition metals such as Fe, Co, Ni, and the M edges of rare earth systems, which are the most prominent elements in magnetic materials. In addition to XMCD contrast, which is used to image ferromagnetic domains, the corresponding X-ray magnetic linear dichroism effect (XMLD) can be used to image antiferromagnetic domains, which has been demonstrated with X-PEEM [33].

The penetrability of soft X-rays through matter, described by the X-ray absorption length, is typically in the few 100 nm regime. Consequently, the transmission geometry in Magnetic TXM (MTXM) permits probing the volume of the specimen up to a few 100 nm in thickness. Although inherently biased toward the near-surface region, these

depths match perfectly most of the magnetic systems of highest current interest, such as thin films or multilayered structures. By contrast, the X-PEEM technique can only probe the magnetic properties within the limited escape depths of the electrons, which in general are restricted to a few nm for photoelectrons and ~5–10 nm for low-energy secondaries, i.e. the surface region in the specimens. The penetration depth of soft X-rays has immediate implications for the sample preparation. Whereas samples for MTXM in transmission geometry have to be prepared on X-ray transparent substrates, similar to TEM substrates such as Si_3N_4 membranes, X-PEEM samples can be deposited on thick substrates, as long as they are conducting, in order to avoid space charges. However, there are recent developments of ion-beam-assisted deposition techniques onto thin membranes, e.g. IBAD MgO [34], which have demonstrated the possibility to grow near-epitaxial thin films for MTXM studies as well.

An additional advantage of MTXM lies in its a pure photon-in/photon-out based technique, such that magnetic fields of in principle any strength and pointing in any direction can be applied during the recording of X-ray images. At the full-field X-ray microscope XM-1, typical magnetic fields up to 2–3 kOe perpendicular to the plane of the sample and up to 1–2 kOe in the plane of the sample can be applied. Thus, samples with both perpendicular and in-plane anisotropy can be investigated. To image in-plane components the sample normal has to be tilted to an direction more perpendicular to the photon beam propagation, thus deteriorating the spatial resolution along the beam direction. Due to X-PEEM being an electron probing technique, it inherently faces severe challenges for applying magnetic fields in arbitrary directions and at higher field values, although certain efforts to compensate the impact of magnetic fields to the electron paths have been demonstrated [35].

The inherently pulsed structure of X-ray synchrotron storage rings permits time-resolved measurements with both MTXM and X-PEEM, i.e. the capability to observe, e.g. fast spin-dynamical processes in magnetic structures. At the ALS, electrons having a typical energy of 1.9 GeV circulate in bunches at a velocity close to the speed of light. The typical bunch length corresponds to about 70 ps, which is also the length of the emitted X-ray flashes. Within a stroboscopic pump-probe scheme, soft X-ray microscopy thus enables studying the spin dynamics on the sub-100 ps time scale in nanoscale magnetic elements. However, the low intensity per bunch prevents single-shot time-resolved imaging and therefore only the perfectly repeatable part of spin-dynamics processes can be studied so far. The various free-electron lasers that are now operating or coming online show promise of single-shot imaging in pump-probe experiments in the future.

To study the microscopic origin of temperature-driven magnetic phenomena, such as the AF to FM phase transition in FeRh and the associated spin-reorientation transition, soft X-ray microscopies can be performed, in principle at both low and elevated temperatures. Recent developments of heating devices on Si_3N_4 membranes, which were designed for use in nanocalorimetry, seems to offer an interesting path for performing MTXM measurements at elevated temperatures [36].

From a historic perspective, the first magnetic soft X-ray images have been reported in 1993, using an X-PEEM system (PEEM-2) at the ALS in Berkeley [24], and the first full-field MTXM images obtained with the TXM at BESSY I in Berlin/Germany were published in 1996 [27].

3. Results and discussion

In the following, we will review some examples from recent research on magnetic structures with nanoscale dimensions, where the imaging capabilities of soft X-ray microscopies were able to provide detailed and unprecedented insight into fundamental physical behavior. Although it might be obvious in most cases, we detail the complementarity of MTXM to other imaging techniques, mostly X-PEEM for each of the following examples.

Vortex structures are found across many length scales extending from cosmological dimensions in galaxies to large tornadoes spanning thousands of kilometers to superconducting materials, where the vortices play a crucial role to allow superconducting wires to be used in future power grids.

Magnetic vortex structures occur in soft ferromagnetic films and patterned elements, such as thin disks of the soft $Ni_{80}Fe_{20}$ alloy, as a result of the balance between exchange and dipolar energies. They are characterized by a curling magnetization in the plane of the disk with a vortex core (VC) in the center, where the magnetization points perpendicular to the plane of the disk. Two binary properties are commonly used to describe this structure: the chirality or better circularity (c), i.e. the counter-clockwise or clockwise curling of the in-plane magnetization, and the polarity (p), i.e. the up or down direction of the vortex core's magnetization. Both the static and dynamic properties of these objects have recently attracted an increased scientific interest both for fundamental and applied reasons. For example, magnetic vortex structures were suggested as potential future high-density and non-volatile recording systems, since the size of the vortex core is proportional to the magnetic exchange length Λ, which can extend into the sub-10 nm regime, and the magnetic core represents a very stable spin configuration, in fact protected by topology.

3.1. Vortex formation

Fig. 4 shows the four different vortex states in a ferromagnetic disk resulting from the combination of the two states for c and p, respectively. They can be separated into two categories with different handedness, which is generally defined as the product of c and p, namely $cp = +1$ or $cp = -1$. All four configurations are degenerate with respect to the total energy. One of the questions which arise is whether the nucleation of those four degenerate states has equal probability [37]. A priori, one would assume that the formation of a magnetic vortex state should exhibit perfect symmetry in this respect, and thus degeneracy. A non-degeneracy would not only constitute an unconventional physical phenomenon at the nanoscale but could also lead to potentially interesting applications of magnetic vortices with regard to magnetic sensor or logic elements. To

experimentally address this topic we have recently imaged with high statistical accuracy a large number of permalloy disk arrays, where vortex states were nucleated by applying a particular magnetic field cycle. The capability of MTXM to image both the in-plane (*c*) and out-of-plane (*p*) components of the spin structures more or less simultaneously (Fig. 5) was crucial for allowing us to observe an asymmetric effect in the formation process of vortex states. In fact, the acquisition speed of MTXM to cover a field of view of about 10 μm in a few seconds only, made it the technique of choice for those studies and superior to any complementary scanning based microscopies, such as SEMPA or STXM. Other full field electron microscopies, such as X-PEEM or Lorentz-TEM would have suffered from the limitations of being able to nucleate the vortex structures from saturated states quickly. The large statistics of MTXM images allowed us to interpret the origin of the experimentally observed asymmetric phenomenon by a combination of an intrinsic Dzyaloshinskii–Moriya interaction (DMI) arising from the spin–orbit coupling [38] and surface-related “extrinsic” factors, including edge defects, surface roughness, etc. Full 3-dim micromagnetic modeling confirmed the experimental data.

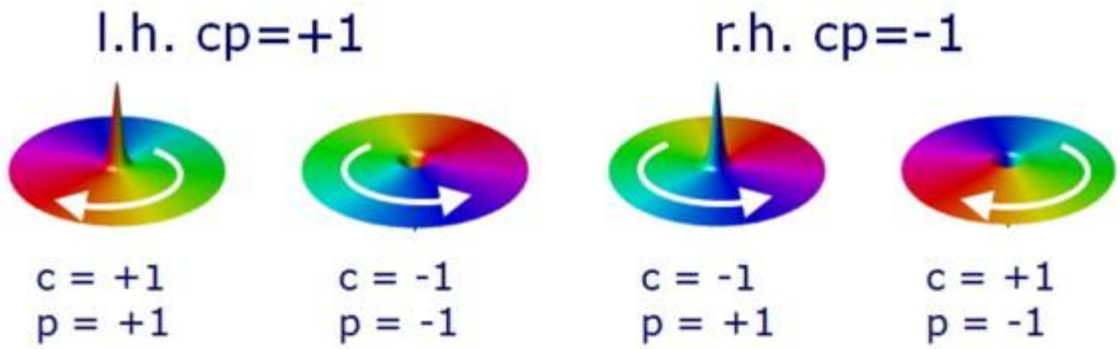

Fig. 4. Schematics of the four different magnetic vortex structure configurations.

Figure options

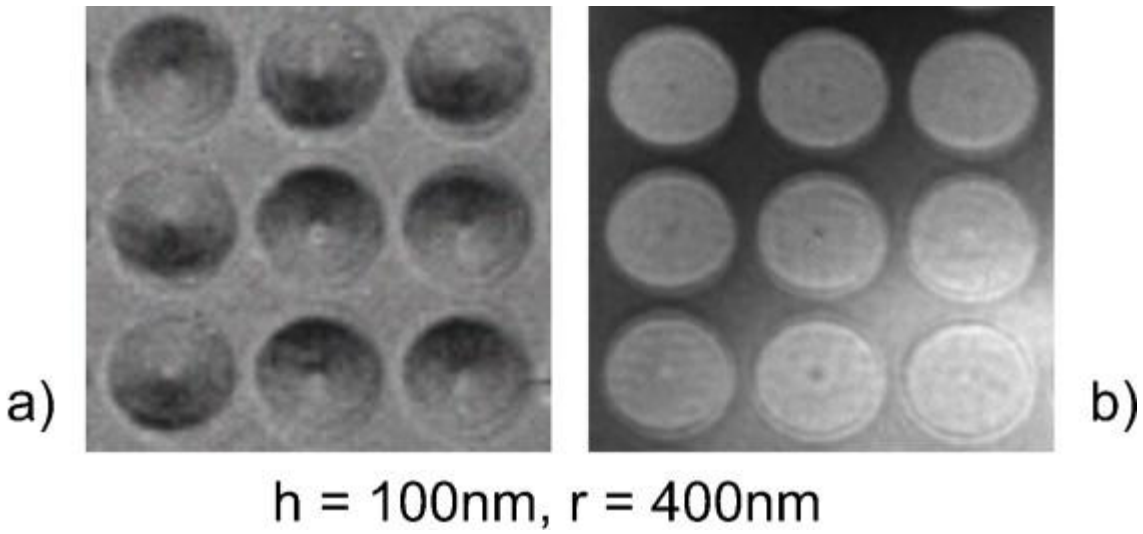

Fig. 5. (a) Magnetic transmission X-ray microscopy (MTXM) image of an array of permalloy dots with thickness h = 100 nm and radius r = 400 nm recorded in a tilted geometry showing (a) the in-plane domain configuration and (b) the same array recorded in a perpendicular geometry imaging the vortex core in the center of the dots.

3.2. Vortex dynamics

Magnetic vortex structures have also been proposed as novel base units for logic devices. Understanding their dynamics requires time-resolved studies with high spatial resolution. Soft X-ray microscopies combine the high spatial resolution with the inherent time structure of current synchrotron storage rings which is less than 100 ps. Since the number of photons per electron bunch at current third generation synchrotrons is rather low, typically only a few tens of photons, a stroboscopic pump-probe scheme has to be used. Hence, about 10^{8-9} pump-probe cycles are required to create a single image, which means that only fully reproducible processes can be studied, or in other words only the fully reproducible part of the magnetization dynamics can be investigated. For details about the experimental setup, see [39].

The results shown in Fig. 6 were obtained at the ALS, operating in the so-called 2-bunch mode operation. Two electron bunches, each 70 ps in length, circulate at a 3 MHz frequency, i.e. they are separated by 328 ns. The clock signal of the synchrotron triggers a fast electronic pulser, which launches fast electronic pulses into a waveguide structure. These pump pulses create a local Oersted field pulse, which initiates a gyrational motion of the vortex structure. The experiment shown in Fig. 6 aimed at investigating the coupling of neighboring vortex structures in arrays of disks with a disk radius of 750 nm. For that purpose, a pair of magnetic disks, labeled “disk 1” and “disk 2” in Fig. 6, was studied. The excitation pulse was acting on “disk 1” only and its gyrational motion can be seen in the sequence of time-resolved MTXM images (Fig. 6a). Through dipolar coupling the neighboring vortex structure (disk 2) is stimulated to start a gyrational motion as well (Fig. 6b), which therefore constitutes a robust new mechanism for energy transfer between spatially separated dipolar-coupled magnetic disks [40]. The detailed motion of both disks, i.e. the x and y components, are displayed in Fig. 6c and e and compared with simulations (Fig. 6d and f). These results clearly show that, in analogy to a system of coupled harmonic oscillators, the two neighboring vortex structures are able to mutually exchange energy and thus can be considered as a new way of information processing or logical base units. Since this process is largely determined by the damping parameter, further developments toward the realization of such devices would require analogous investigations on materials with low damping.

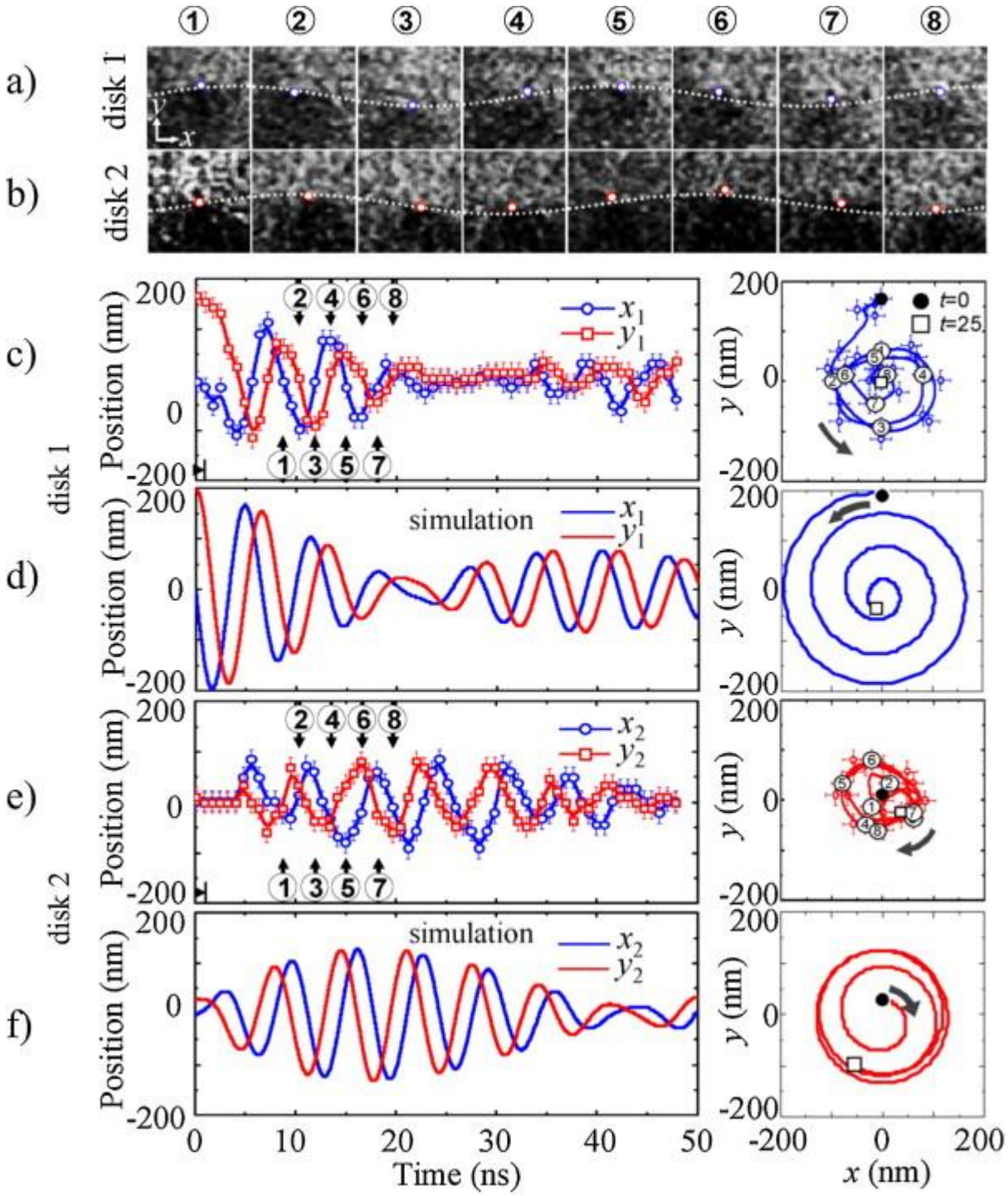

Fig. 6. MTXM study of vortex-core gyrations in two dipolar-coupled Py disks (disk 1 and disk 2), with only disk 1 in (a) being excited by an applied field. Experimental images showing the motion of the vortex cores in the center of the circular disk (a and b), extracted gyrational motion trajectories (c and e) and comparison with simulations (d and f).

From Ref. [40].

Studies of the dynamics are crucial to develop new functionalities and therefore time resolved magnetic microscopies have been a major focus in the recent past. X-ray based microscopies, such as MTXM, STXM [41], and X-PEEM [42] utilizing the inherent time structure of synchrotron radiation have all been expanded over the last decade to allow such studies. Their main advantage is that they combine both good spatial resolution and temporal resolution. There are other techniques with higher spatial resolution or better time resolution, but it is the combination of both, which makes X-ray microscopies unique for those studies.

3.3. Adding depth resolution to X-ray microscopies

Although magnetic thin films are a priori considered to be 2-dim spin systems, the 3rd dimension often plays a quite important role and will increasingly become even more important in the future. Examples are magnetic multilayers, where the depth-dependence of the magnetization or the spin character at buried interfaces is a very interesting topic to study [43]. Other examples where the 3rd dimension plays an important role are magnetic nanoparticles [44], core–shell structures, such as hard/soft materials for future permanent magnet materials [45], or magnetic supercrystals. The latter ones are arrays of nanocrystals, which self-assemble into superlattices. They are expected to exhibit unique size-dependent electronic, optical and magnetic properties which can be easily altered [46]. In particular, magnetic nanoparticle arrays of sizes of 15 nm or below in all dimensions (Fig. 7) attract growing interest because of their potentials for studying the fundamentals of nanoscale magnetism and for novel technological applications. Although particles of such size are usually in a single-domain state, there is a size-, structure-, and temperature-dependent nanoscale magnetism, which scales with particle volume and intrinsic magnetic constants, such as anisotropy. Tuning the interparticle distance is one way to tailor the behavior of such supercrystals (inset of Fig. 7). Finally, in order to increase many-fold the performance of future memory and logic devices, new concepts for magnetic media also foresee 3-dim structures [47] and [48].

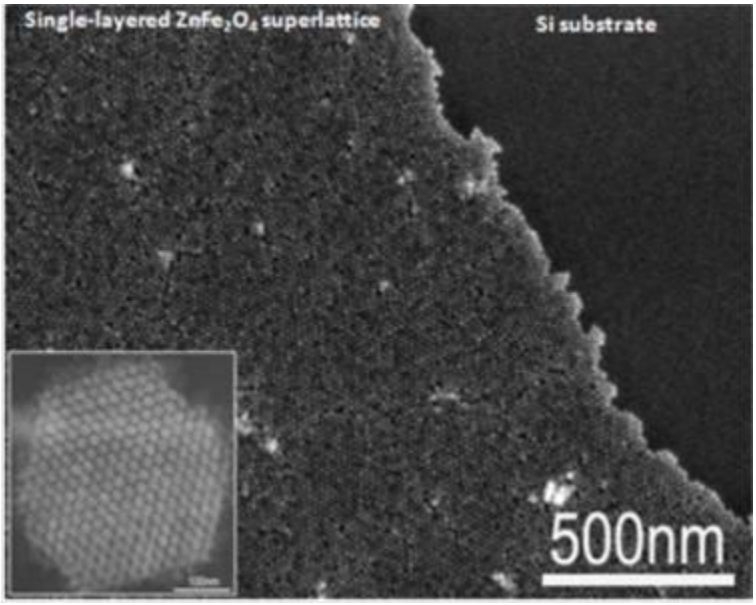

Fig. 7. Scanning electron microscope (SEM) image of a 2-D superlattice self-assembled from 15-nm $ZnFe_2O_4$ nanocrystals. Inset shows a transmission electron microscope (TEM) of 3-D $ZnFe_2O_4$ supercrystals.

Therefore magnetic imaging capabilities in three dimensions have received increased interest recently. Soft X-ray microscopies offer various ways to approach this. One way is to perform computational tomography, which requires a set of projection images recorded at varying projection angle. From those projections, one can reconstruct the full three-dimensional information. So far, this technique has been successfully demonstrated and is being used now as a standard application for the high-resolution nanotomography of whole cells [49].

Another approach to obtain depth-resolved information is based on excitation with soft X-ray standing waves (SW) generated by Bragg reflection from a multilayer mirror substrate. The interference between incoming and reflected X-ray wavefronts generates a standing wave inside the multilayer. This standing wave can then be moved vertically through the sample by varying either the photon energy around the Bragg condition, the angle of incidence of the incoming wavefront, or by moving the X-ray spot across a sample in which one layer has a wedge profile [50] and [51]. Photoemission intensities which are recorded as a function of the incoming photon energy, incidence angle or spot position then permit quantitatively deriving the depth-resolved film structure of the sample by comparing the intensities to X-ray optical theory calculations [52]. The combination of this depth-resolved method, e.g. with a lateral information from X-PEEM, thus provides a three-dimensional representation of the magnetic structures inside the specimen. Proof-of-principle standing-wave experiments were conducted at the elliptically polarized soft X-ray undulator beamline UE49-PGM-a at the storage ring BESSY-II in Berlin/Germany. This microfocus beamline is equipped with an Elmitec PEEM-III endstation with an integrated photoelectron energy analyzer (Fig. 8, left panel). The experimental geometry allowed for photon incidence angles between 13.8° and 17.8°, as measured from the sample surface plane. For the particular multilayer

substrate and for the incidence angle range of 13.8–17.8°, the Bragg condition was achieved by using a photon energy range between 663 eV and 516 eV, respectively. As confirmed from simulations of electron spectra, the combination of photon energies of 620–750 eV and a grazing angle of 13.8° yields the best resolved Co 3p, Al 2p, Si 2p and C 1s photoemission spectra, unobstructed by any constant-kinetic-energy Auger electron features, and permits scanning the SW through the sample. Fig. 9 shows the results of such an X-PEEM experiment utilizing the standing wave approach, in which depth resolution was added to the lateral information of X-PEEM in a nanostructured system consisting of square arrays of circular magnetic Co nanodots, as shown in Fig. 8, right panel. They were nominally 4 nm in thickness and 1 μm in diameter and were grown on a [23.6 Å-Si/15.8 Å-Mo] × 40 multilayer substrate to act as the standing wave generator. Fig. 9 displays the various core levels (Al 2p, Si 2p, C 1s, and Co 3p) captured at a photon energy of 680 eV, which is the energy where the intensity of the Al 2p line for the aluminum atoms around the Co dots is maximum. Varying the photon energy over the Bragg condition of the multilayer reveals a winking on and off of these images that is characteristic of the depth of each species below the surface. Comparing the experimental results to X-ray optical simulations then permitted determining the detailed depth profiles of all species present. To obtain magnetic sensitivity in depth, the next step is to exploit magnetic dichroism in core-level photoemission with polarized X-rays.

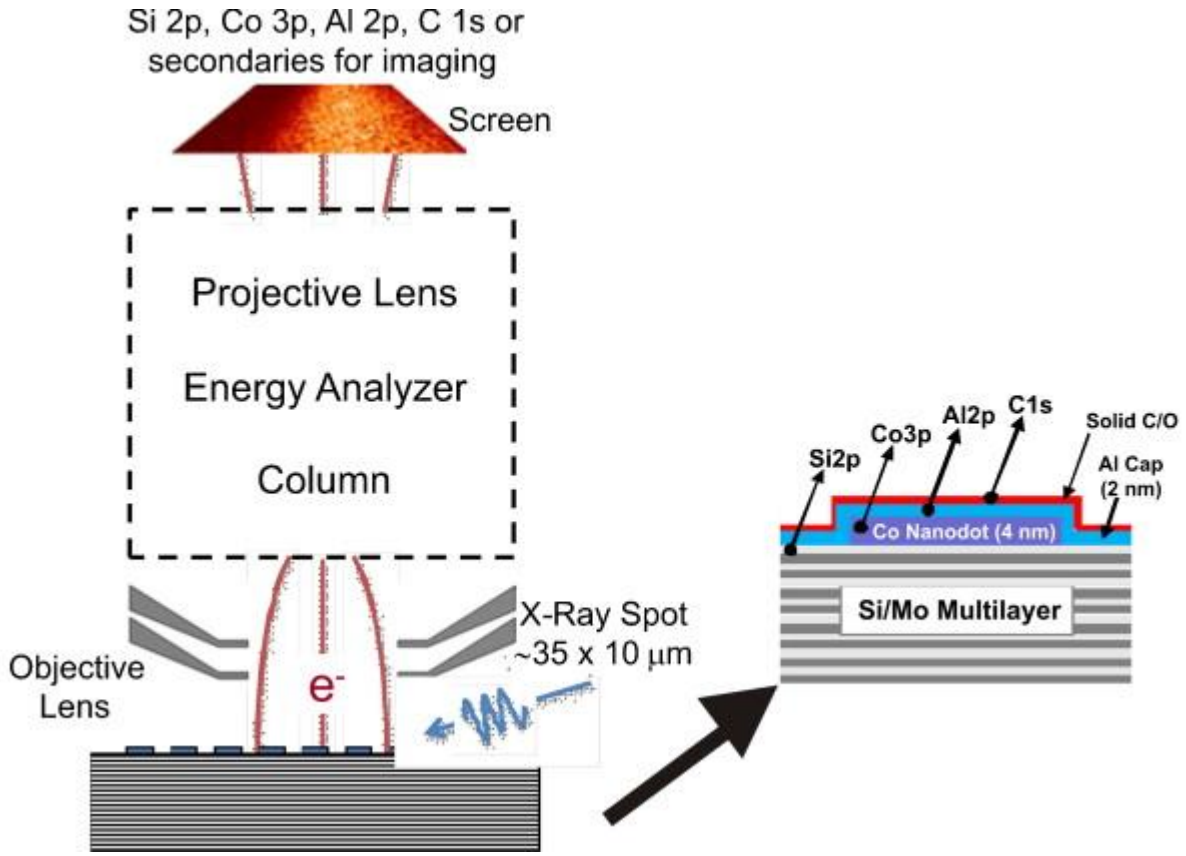

Fig. 8. (Left panel) Schematic diagram of the experimental setup including the sample and the Elmitec PEEM endstation at the elliptically polarized soft X-ray undulator beamline UE49-PGM-a at the storage

ring BESSY-II. (Right panel) Cross-sectional as-grown schematic of the Co microdot structure, with the photoemission core peaks used in the element-specific study of the constituents of the structure indicated by arrows.

From Ref. [50].

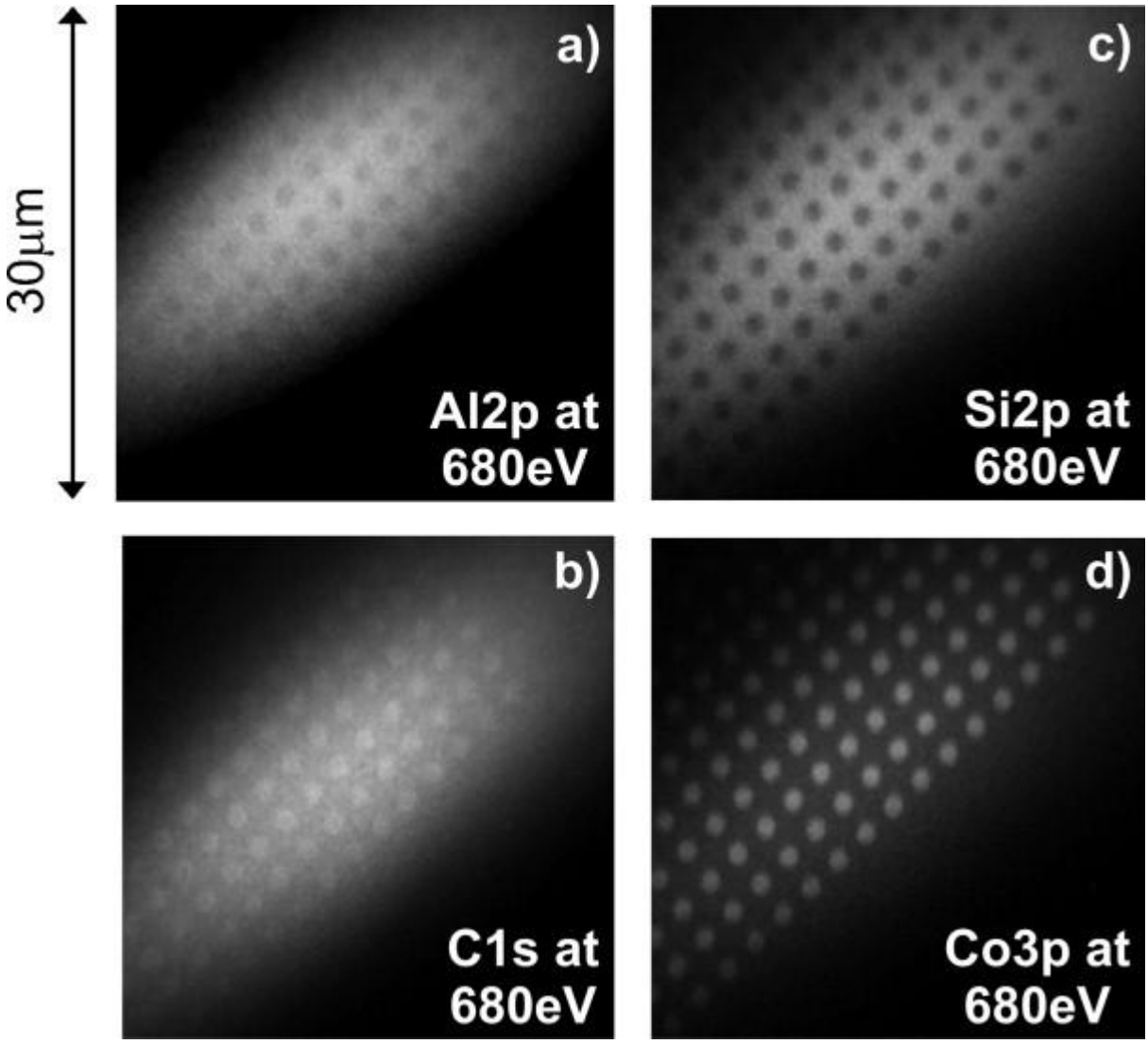

Fig. 9. Standing-wave X-PEEM images from the sample in Fig. 8 captured at *hv* = 680 eV for (a) Al 2p, (b) C 1s, (c) Si 2p and (d) Co 3p core levels. 680 eV is the energy for which the Al image is a maximum off the microdots.

From Ref. [50].

The aforementioned example utilized the X-PEEM technique with energy filtering to obtain depth resolved information. However, the standing wave approach is not limited to this imaging technique. MTXM can be operated in principle in reflection mode [53], which then could detect also the reflected X-ray intensity of a standing wave generated in a multilayer substrate. Advantages for the pure photon based MTXM in terms of the

capability to investigate the depth resolved magnetization as a function of applied magnetic fields are easy to envision.

3.4. Varying the sample environment: temperature

Another important parameter in magnetic X-ray microscopies is the capability to vary the temperature at the sample. This will allow not only to investigate, e.g. the microscopic origin of the transition from a ferromagnetic to a paramagnetic phase by approaching the Curie temperature, but also to address the vast area of spin-thermal effects in spin-caloritronics. This latter field has recently launched a plethora of scientific studies both from a most basic physics point of view but also for potential applications, for example, in reduced energy-consumption devices. For an overview on spincaloritronics, see [54]. A precise control of the local temperature at the specimen, a large temperature range, and a controllable temperature gradient are essential for such studies. One approach is to integrate a heating element onto an X-ray transparent amorphous Si–N membrane using standard microfabrication techniques. Fig. 10a and b shows one such device with a non-inductive double-spiral Pt heater. This device has been shown to provide a highly uniform temperature over the sample area in the typical atmospheric environment of a MTXM and therefore enables temperature dependent studies [55]. Results from a proof-of-principle experiment on a 30 nm thin Ni film, which was imaged below (320 °C) and above (400 °C) the Curie temperature, are shown in Fig. 10c. Note that this measurement was performed with a slightly different heater design (nanocalorimeter [36]). As expected, the magnetic domains disappear above T_c, which also proves that such heating devices allow to reach several hundreds of °C with very small power input and short amount of time. The temperature can be cycled several times without showing any degradation of the device.

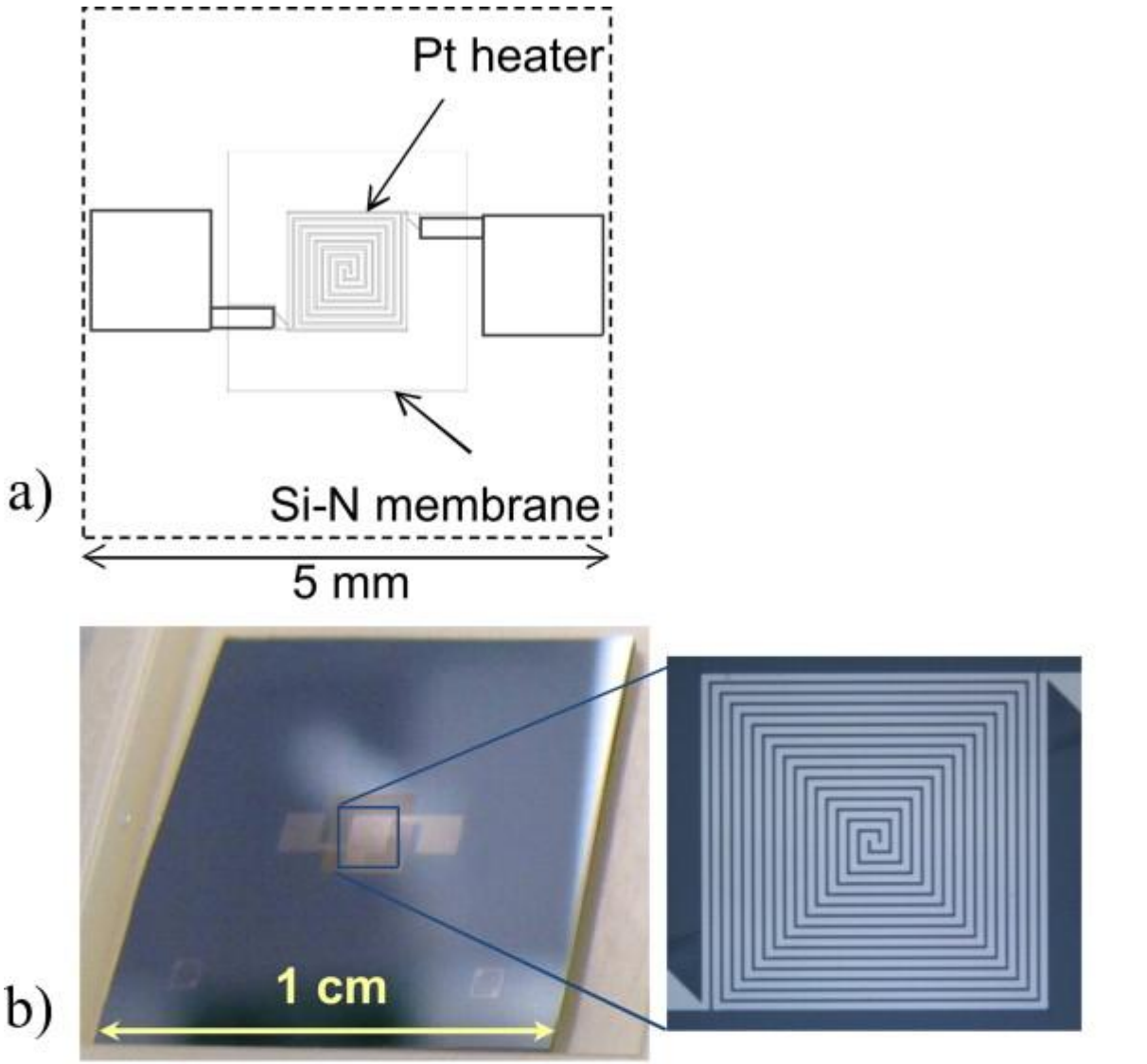
Pt heater
a)
Si-N membrane
5 mm
b)
1 cm
c)
2 μm
~400°C (T>T$_C$)
~320°C (T<T$_C$)

Fig. 10. (a) Schematic diagram of the top view of a microfrabricated amorphous Si–N membrane-based heater stage. (b) Picture of an actual heater stage, fitting on a 1 cm × 1 cm Si chip. The right panel shows a zoomed in detail of the double spiral Pt heating element. (c) Proof of principle images of a Ni film heated through its Curie temperature, showing no ferromagnetic domains above T_c and long micron size domains below T_c. These images were obtained on a membrane-based heating device similar to (a) and (b) [36].

We end this section by noting that the variation of temperature in an X-ray microscope is not inherently a unique capability; however, if such microscopes could only operate at ambient conditions, the unique combination of high spatio-temporal resolution with inherent elemental specificity would still leave out a large fraction of interesting science, particularly in the realm of magnetic materials.

4. Conclusions

Understanding fundamental properties in magnetic materials requires detailed information on the nanometer length scale, but with obvious extensions now into the mesoscale to address complex and correlated behavior as well as non-deterministic properties and functionality. Full-field soft X-ray microscopies, such as MTXM and X-PEEM are well suited to provide unique, element-specific and quantitative magnetic information over a large field of view with high spatial resolution reaching into the 10 nm regime.

In the near term future, those techniques will also be able to provide full three-dimensional information and, with the new X-ray sources which are starting operation now, these methods will within the next decade be able to study fundamental magnetic time scales.

Acknowledgements

This work was supported by the Director, Office of Science, Office of Basic Energy Sciences, Materials Sciences and Engineering Division, of the U.S. Department of Energy under contract no. DE-AC02-05-CH11231 and by Leading Foreign Research Institute Recruitment Program through the National Research Foundation (NRF) of Korea funded by the Ministry of Education, Science and Technology (MEST) (2012K1A4A3053565).

We want to thank the many colleagues for longstanding and fruitful collaborations, in particular W.L. Chao, E. Anderson, F. Salmassi, E.M. Gullikson (CXRO), K. Yamada, T. Ono (U Kyoto), S. Kasai (NIMS Tsukuba), T. Sato, Y. Nakatani (U Chofu), G. Meier, A. Vogel, L. Bocklage, (U Hamburg Germany), H. Jung, K.-S. Lee, D.-E. Jeong, Y.-S. Choi, Y.-S. Yu, D.-S. Han, S.K. Kim, (Seoul Natl U Korea), A.X. Gray (UC Davis), F. Kronast (HZB Berlin), Ch. Papp (U Erlangen), S.-H. Yang (IBM Almaden), S. Cramm, I.P. Krug, C.M. Schneider (Juelich), H.A. Dürr (SLAC). A special thanks also goes to the staff of CXRO, ALS, BESSY.

References

1 S.D. Bader, S.S.P. Parkin, Annu. Rev. Condens. Matter Phys., 1 (2010), pp. 71–88
2 J. Stoehr, H.C. Siegmann, Magnetism, Springer, Berlin/Heidelberg (2006)
3 M. Baibich *et al.,* Phys. Rev. Lett., 61 (1988), pp. 2472–2475
4 G. Binasch, P. Grünberg, F. Saurenbach, W. Zinn, Phys. Rev. B, 39 (1989), pp. 4828–4830
5 See "Celebrating 20 years of GMR – past, present and future", AAPPS Bull. 18 (5–6) (2008).
6 D.C. Ralph, M.D. Stiles, J. Magn. Magn. Mater., 320 (2008), pp. 1190–1216
7 See e.g. http://www.everspin.com/PDF/ST-MRAM_Technical_Brief.pdf.
8 N.A. Spaldin, M. Fiebig, Science, 309 (2005), pp. 391–392
9 T. Zhao, A. Scholl, F. Zavaliche, K. Lee, M. Barry, A. Doran, M.P. Cruz, Y.H. Chu, C. Ederer, N.A. Spaldin, R.R. Das, D.M. Kim, S.H. Baek, C.B. Eom, R. Ramesh, Nat. Mater., 5 (2006), p. 823
10 N. D'Souza, J. Atulasimha, S. Bandyopadhyay, J. Phys. D: Appl. Phys., 44 (2011), p. 265001
11 D.T. Attwood, Soft X-rays and Extreme Ultraviolet Radiation: Principles and Applications, Cambridge University Press, Cambridge (1999)
12 J. Kerr, Philos. Mag., 3 (5) (1877), pp. 321–343
13 M. Faraday, Philos. Trans. R. Soc. (London), 136 (1846), pp. 1–20
14 C.T. Chen, F. Sette, Y. Ma, S. Modesti, Phys. Rev. B, 42 (1990), pp. 7262–7265
15 .T. Thole, P. Carra, F. Sette, G. van der Laan, Phys. Rev. Lett., 68 (1992), pp. 1943–1946
16 P. Carra, B.T. Thole, M. Altarelli, X. Wang, Phys. Rev. Lett., 70 (1993), pp. 694–697
17 See http://www.whitehouse.gov/mgi.
18 A. Hubert, R. Schäfer, Magnetic Domains: The analysis of Magnetic Microstructure, Springer-Verlag, Berlin (1998)
19 H.J. Williams, F.G. Foster, E.A. Wood, Phys. Rev., 82 (1951), p. 119
20 J.P. Park, P. Eames, D.M. Engebretson, J. Berezovsky, P.A. Crowell, Phys. Rev. B, 67 (2003), p. 020403
21 J.N. Chapman, J. Phys. D: Appl. Phys., 17 (1984), p. 623
22 J. Unguris, G. Hembree, R.J. Celotta, D.T. Pierce, J. Magn. Magn. Mater., 54 (1986), p. 1629
23 E. Bauer, Rep. Prog. Phys., 57 (1994), p. 895
24 J. Stoehr, Y. Wu, B.D. Hermsmeier, M.D. Samant, G.R. Harp, S. Koranda, D. Dunham, B.P. Tonner, Science, 259 (1993), pp. 658–661
25 Y. Martin, H.K. Wickramasinghe, Appl. Phys. Lett., 50 (1987), p. 1455
26 R. Wiesendanger, H.-J. Güntherodt, G. Güntherodt, R.J. Gambino, R. Ruf, Phys. Rev. Lett., 65 (1990), p. 247
27 P. Fischer, G. Schütz, G. Schmahl, P. Guttmann, Z. Phys. B, 101 (1996), pp. 313–316
28 The 10th International Conference on X-ray Microscopy, AIP Conference Proceedings 1365, http://scitation.aip.org/proceedings/confproceed/1365.jsp.

29 W. Chao, P. Fischer, T. Tyliszczak, S. Rekawa, E. Anderson, P. Naulleau, Opt. Express, 20 (9) (2012), pp. 9777–9783
30 P. Fischer, D.-H. Kim, W. Chao, J.A. Liddle, E.H. Anderson, D.T. Attwood, Mater. Today, 9 (2006), pp. 26–33
31 X.M. Cheng, D.J. Keavney, Rep. Prog. Phys., 75 (2012), p. 026501
32 P. Guttmann, C. Bittencourt, S. Rehbein, P. Umek, X. Ke, G. Van Tendeloo, C.P. Ewels, G. Schneider, Nat. Photon., 6 (2012), pp. 25–29
33 A. Scholl, J. Stoehr, J. Luening, J.W. Seo, J. Fompeyrine, H. Siegwart, J.-P. Locquet, F. Nolting, S. Anders, E.E. Fullerton, M.R. Scheinfein, H.A. Padmore, Science, 287 (2000), p. 1014
34 D.W. Cooke, F. Hellman, J.R. Groves, B.M. Clemens, S. Moyerman, E.E. Fullerton, Rev. Sci. Instrum., 82 (2011), p. 023908
35 F. Kronast, J. Schichting, F. Radu, S.K. Mishra, T. Noll, H.A. Duerr, Surf. Interface Anal., 42 (2010), p. 1532
36 D.R. Queen, F. Hellman, Rev. Sci. Instrum., 80 (2009), p. 063901
37 M.-Y. Im, P. Fischer, Y. Keisuke, T. Sato, S. Kasai, Y. Nakatani, T. Ono, Nat. Commun., 3 (2012), p. 983
38 A.B. Butenko, A.A. Leonov, A.N. Bogdanov, U.K. Rößler, Phys. Rev. B, 80 (2009), p. 134410
39 S. Kasai, P. Fischer, M.-Y. Im, K. Yamada, Y. Nakatani, K. Kobayashi, H. Kohno, T. Ono, Phys. Rev. Lett., 101 (2008), p. 237203
40 H. Jung, K.-S. Lee, D.-E. Jeong, Y.-S. Choi, Y.-S. Yu, D.-S. Han, A. Vogel, L. Bocklage, G. Meier, M.-Y. Im, P. Fischer, S.-K. Kim, NPG Sci. Rep., 1 (2011), p. 59
41 Y. Acremann, J.P. Strachan, V. Chembrolu, S.D. Andrews, T. Tyliszczak, J.A. Katine, M.J. Carey, B.M. Clemens, H.C. Siegmann, J. Stoehr, Phys. Rev. Lett., 96 (2006), p. 217202
42 S.-B. Choe, Y. Acremann, A. Scholl, A. Bauer, A. Doran, J. Stoehr, H.A. Padmore, Science, 304 (2004), p. 420
43 C.S. Fadley, J. Electron Spectrosc. Relat. Phenom., 178 (2010), p. 2
44 F. Kronast, N. Friedenberger, K. Ollefs, S. Gliga, L. Tati-Bismaths, R. Thies, A. Ney, R. Weber, C. Hassel, F.M. Roemer, A.V. Trunova, C. Wirtz, R. Hertel, H.A. Duerr, M. Farle, NanoLetters, 11 (2011), p. 1710
45 P.K. Sahota, Y. Liu, R. Skomski, P. Manchanda, R. Zhang, M. Franchin, H. Fangohr, G.C. Hadjipanayis, A. Kashyap, D.J. Sellmyer, J. Appl. Phys., 111 (2012), p. 07E345
46 D.V. Talapin, J.-S. Lee, M.V. Kovalenko, E.V. Shevchenko, Chem. Rev., 110 (2010), pp. 389–458
47 R. Lavrijsen, J.-H. Lee, A. Fernandez-Pacheco, D.C.M.C. Petit, R. Mansell, R.P. Cowburn, Nature, 493 (2013), p. 647
48 S.S.P. Parkin, M. Hayashi, L. Thomas, Science, 320 (2008), pp. 190–194
49 G. Schneider, E. Anderson, S. Vogt, C. Knoechel, D. Weiss, M. Legros, C. Larabell, Surf. Rev. Lett., 9 (2002), p. 177
50 F. Kronast, R. Ovsyannikov, A. Kaiser, C.C. Wiemann, S.-H. Yang, D.-E. Bürgler, R.R. Schreiber, F. Salmassi, P. Fischer, H.A. Dűrr, C.M. Schneider, W. Eberhardt, C.S. Fadley, Appl. Phys. Lett., 93 (2008), pp. 243116–243123

51 A.X. Gray, F. Kronast, Ch. Papp, S.-H. Yang, S. Cramm, I.P. Krug, F. Salmassi, E.M. Gullikson, D.I. Hilken, E.H. Anderson, P. Fischer, H.A. Dürr, C.M. Schneider, C.S. Fadley, Appl. Phys. Lett., 97 (2010), pp. 062503–062513
52 S.-H. Yang, A.X. Gray, A.M. Kaiser, B.S. Mun, J.B. Kortright, C.S. Fadley, J. Appl. Phys., 113 (2013), p. 073513 The software package for calculating such effects, the Yang X-ray Optics (YXRO) program, is available at: https://sites.google.com/a/lbl.gov/yxro/home
53 G. Denbeaux, P. Fischer, F. Salmassi, K. Dunn, J. Evertsen, S. Aoki, Y. Kagoshima, Y. Suzuki (Eds.), Proceedings of the 8th International Conference on X-ray Microscopy, IPAP Conf. Series 7 (2006), pp. 375–386
54 G. Bauer, E. Saitoh, B.J. van Wees, Nat. Mater., 11 (2012), p. 391
55 C. Baldasseroni, D.R. Queen, D.W. Cooke, K. Maize, A. Shakouri, F. Hellman, Rev. Sci. Instrum., 82 (2011), p. 093904

DISCLAIMER